JOURNAL OF SPACECRAFT AND ROCKETS
Vol. 45, No. 6, November–December 2008

Engineering Notes

ENGINEERING NOTES are short manuscripts describing new developments or important results of a preliminary nature. These Notes should not exceed 2500 words (where a figure or table counts as 200 words). Following informal review by the Editors, they may be published within a few months of the date of receipt. Style requirements are the same as for regular contributions (see inside back cover).

Global Static Testing and Model Validation of Stiffened Thin-Film Polyimide Panels

Jonathan T. Black*
Air Force Institute of Technology, Wright–Patterson Air Force Base, Ohio 45430
Jack Leifer†
Trinity University, San Antonio, Texas 78212
and
Suzanne Weaver Smith‡
University of Kentucky, Lexington, Kentucky 40506

DOI: 10.2514/1.37131

Nomenclature

E_{app}	=	apparent modulus of a hollow beam
E_s	=	modulus of elasticity for the solid material
E_x	=	modulus of elasticity along the major axis
E_y	=	modulus of elasticity along the minor axis
E_1	=	modulus of elasticity along the 1 axis
E_2	=	modulus of elasticity along the 2 axis
G_{12}	=	shear modulus
l	=	hexagon edge length
t	=	hexagonal void spacing
ε_i	=	strain along the i axis
θ	=	internal angle of the hexagon
ν_{ij}	=	generic Poisson's ratio
ρ	=	volumetric density
σ_i	=	stress along the i axis

I. Introduction

STIFF thermal-formed thin-film polyimide panels are part of a unique class of structures that seek to mitigate some of the modeling and testing complications presented by other flexible and highly nonlinear ultralightweight membrane structures. A detailed static characterization of these panels is essential to ensure optimal performance in a variety of applications. This Note examines the global static behavior of stiff thermal-formed thin-film polyimide panels and validates novel numerical models that capture the behavioral mechanics of the panels. The work presented here is a continuation of the work presented by Black et al. [1,2] and is part of an overall effort to characterize static and dynamic behavior of these panels [3].

Although inflatable and/or rigidizable space structures have recently been extensively investigated [4–6], formed or stiffened membrane structures have received substantially less attention. Flint et al. [7,8] examined doubly curved form-stiffened thin-film shells in which the membrane is manufactured such that, without adding mass, the final surface had permanent depth and curvature. Song et al. [9] investigated a membrane torus with a 1.8 m ring diameter and a 0.2 m tube diameter. Unlike similar tori investigated by Griffith and Main [10] and Ruggiero et al. [11], a regular pattern of convex hexagonal domes (8 mm side to side and 3.5 mm high) was formed into the polyimide film from which the torus was constructed. These domes provide the stiffness that enables the structure to be self-supporting and are comparable with the tessellating thermal-formed honeycomb pattern that provides the stiffness of the polyimide panels examined here.

In small-scale compression testing of the panels, significant nonlinear stiffness behavior was observed. To model this behavior, the stiffness of nonlinear springs was previously defined to match that measured experimentally, producing models that quite faithfully replicated experimental data. Modeling full-sized panels with this approach, however, also yields model sizes on the order of hundreds of thousands of degrees of freedom, requiring significant computational effort [1–3]. Because of the disappearance of the observed small-scale local nonlinear behavior at the full-panel scale described here, the use of linear shell element models is appropriate. An alternate modeling approach is therefore proposed in which the internal honeycomb structure is approximated in apparent material properties and the panels are assumed to be solid plates that can be coarsely meshed, eliminating the need for finely meshed models that are hundreds of thousands of degrees of freedom in size or for experimental data used in the previous studies.

Static bending tests on two different panels are described here, along with the formulation of the apparent material properties. Simple coarsely meshed finite element models that do not require detailed modeling of the internal honeycomb geometry of the panels are then validated with experimental data.

II. Panel Experimental Data

Investigation of the global macroscale static behavior of the panels was undertaken in the form of panel bending tests. Two rectangular panels (25.0825 × 26.67 × 1.905 cm) were tested using the setup shown in Fig. 1. One panel was manufactured from 0.127-mm-thick (0.005 in.) polyimide film and the other was manufactured from 0.0762-mm-thick (0.003 in.) polyimide film. Each panel was supported along parallel edges by the edge-support dowels that were fully constrained to approximate a simple two-dimensional line-contact support along the panel edges. Several different loads were applied to the center of each panel, and the displacement of two points along the centerline of the panel were recorded for each load by the Keyence laser displacement sensors (capable of resolving displacements greater than 10 μm) and data acquisition system, shown in Fig. 1. The nodes (defined as junctions of the sidewalls of

Presented as Paper 2137 at the 49th AIAA/ASME/ASCE/AHS/ASC Structures, Structural Dynamics, Schaumburg, IL, 7–10 April 2008; received 13 February 2008; revision received 12 May 2008; accepted for publication 25 July 2008.

*Assistant Professor, Department of Aeronautics and Astronautics. Member AIAA.
†Assistant Professor, Department of Engineering Science, One Trinity Place. Member AIAA.
‡Lester Professor of Mechanical Engineering, 151 Ralph G. Anderson Building. Associate Fellow AIAA.

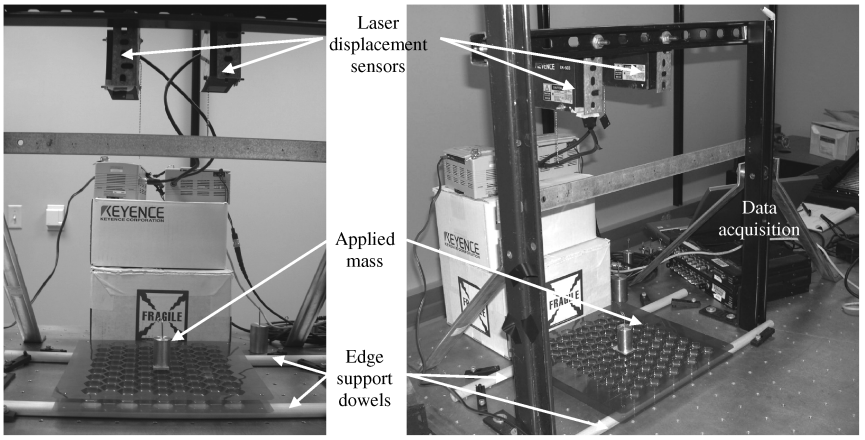

Fig. 1 Rectangular panel bending test setup.

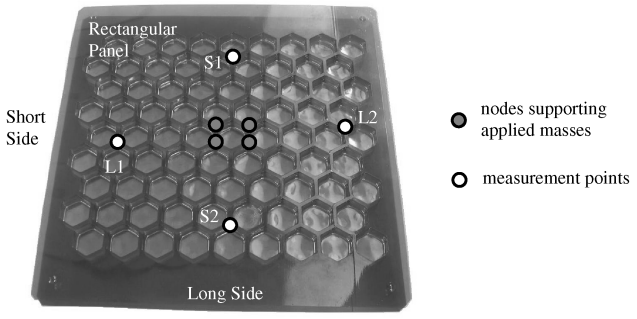

Fig. 2 Rectangular, stiff, ultralightweight polyimide panel with relevant loading and measurement points marked.

the honeycomb) that supported the applied loads and the nodes at which displacement was measured are shown in Fig. 2. Each rectangular panel was tested under two support conditions: one in which the long sides of the panels were supported by the edge-support dowels and the short sides were free and one in which the short sides of the panels were supported by the edge-support dowels and the long sides were free. In the long-side-supported configuration, displacements were measured at points L1 and L2; in the short-side-supported configuration, displacements were measured at points S1 and S2, shown in Fig. 2.

To mitigate the possibility of systemic bias arising from mechanical hysteretic effects caused by repeated bending in the same direction or misalignments, three different groups of full-panel bending tests were undertaken for each of the long-side-supported and short-side-supported test configurations. After several initial sets of data were taken, the panels were rotated 180 deg, switching the positions of the measurement points, and flipped upside down so that bending occurred in the opposite direction. Figures 3 and 4 show the results of the experimental bending tests for the stiff ultralightweight panels manufactured from 0.127-mm-thick (0.005 in. or 5 mil) and 0.0762-mm-thick (0.003 in. or 3 mil) polyimide film, respectively. In both of the figures, the upper-left graph shows the 0 deg or initial data group, the upper-right graph shows the data from the same panels rotated 180 deg, the bottom-left graph shows the data from the same panels flipped upside down, and the bottom-right graph shows all of the data in the previous three graphs plotted together with fit trend

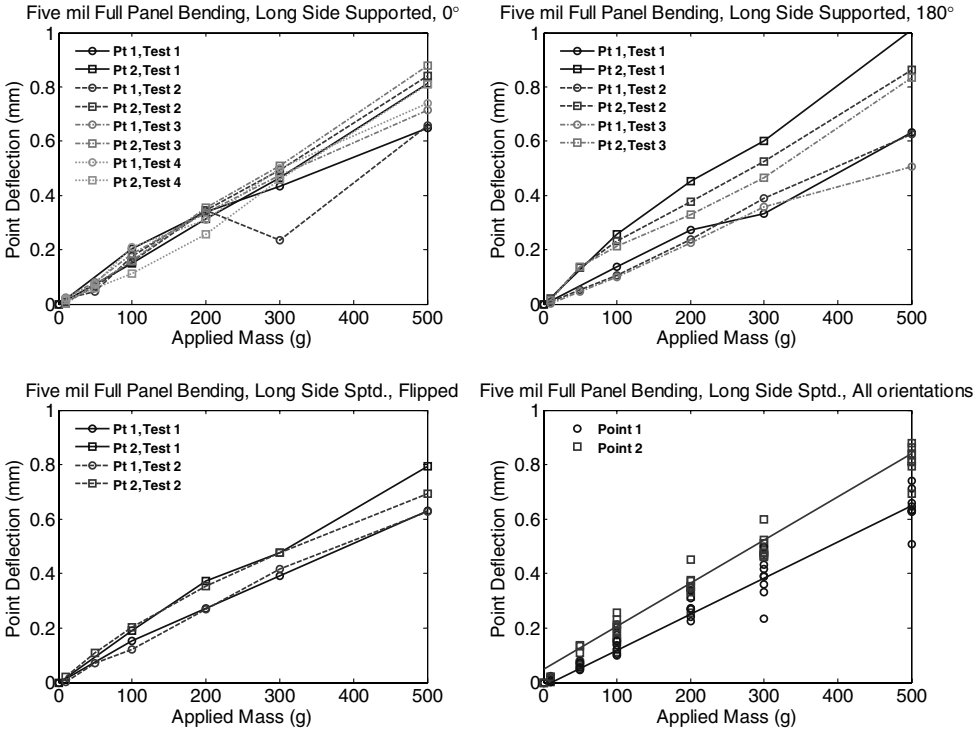

Fig. 3 Long-side-supported full-panel bending data for the panel manufactured from 0.127 mm (5 mil) polyimide film.

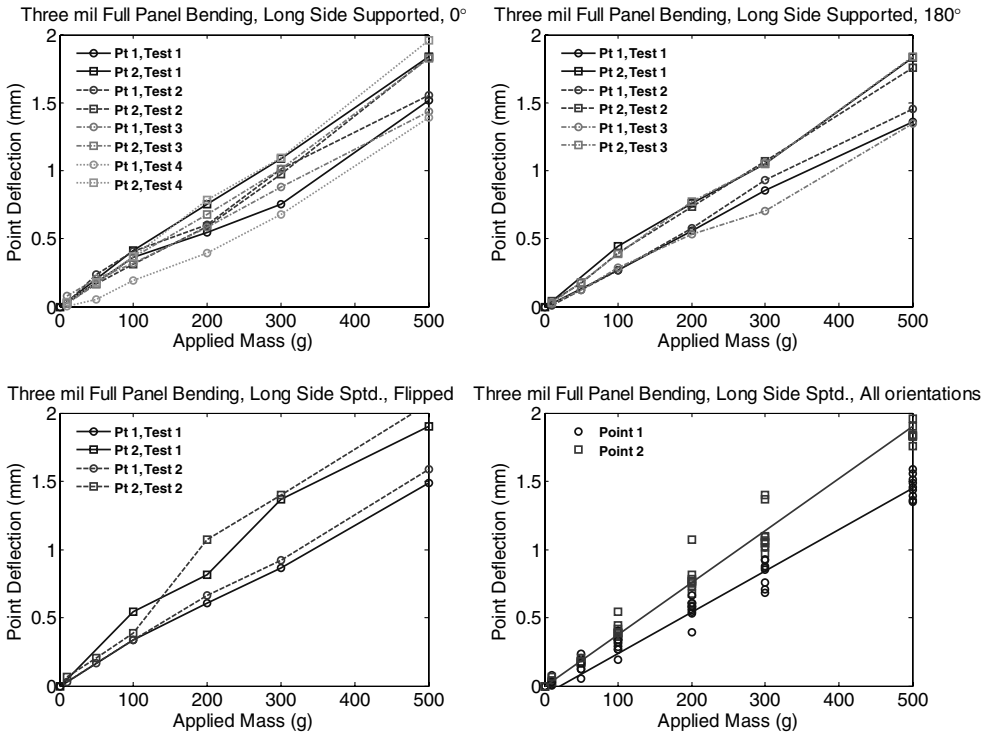

Fig. 4 Long-side-supported full-panel bending data for the panel manufactured from 0.0762 mm (3 mil) polyimide film.

lines (note that experimental variation causes the trend lines to indicate small erroneous nonzero displacements at zero load). Points 1 and 2 in the graphs in Figs. 3 and 4 correspond to measurement points L1 and L2 in Fig. 2, with the rotation or flip accounted for.

Figures 3–5 show the deflection of each measured point as a function of the applied mass. They demonstrate that in bending, the panels behave, in general, in a linear fashion, regardless of their orientation. Figures 3 and 4 also show that point 2 consistently demonstrates greater deflection than point 1. Because this disparity is present regardless of orientation, and taking into account that point 1 is slightly closer to the center of the panel than point 2 (Fig. 2), it is likely that the panels under point loading deform into a saddle configuration, with curvature in both the x and y directions, rather than a simple trough configuration as predicted by classical plate-bending theory [12,13]. For this reason, two trend lines are fit to the data shown in the lower-right graphs in Figs. 3 and 4. The upper line fits the deflection of point 2 and the lower point 1. These lines will be compared with the results of the finite element models in the next section.

Comparing Figs. 3 and 4 demonstrates the effect of varying the thickness of the polyimide film from which the panels are manufactured. The figures show the bending test results from rectangular panels that are identical in every way with the exception of the thickness of the polyimide film. As expected, the panel manufactured from the thinner 0.0762 mm film in Fig. 4 exhibits greater deflection under the same loading than the thicker 0.127 mm film panel in Fig. 3. But although the overall panel stiffness of the 0.0762 mm panel is shown to be less than the 0.127 mm, it still behaves in a similar linear fashion for the same range of loads.

Figure 5 provides a side-by-side comparison of the two different rectangular panels in bending with their short sides supported. The graphs on the left side of the figure show the deflection of points 1 and 2, corresponding to S1 and S2 in Fig. 2, of the panel manufactured from 0.127-mm-thick film and the graphs on the right of the figure show the deflection of the same points of the 0.0762-mm-thick film panel. The plot scales are identical to allow a direct comparison of the panels' deflection. As expected, the panel manufactured from the thinner 0.0762 mm film exhibits greater deflection under the same loading than the thicker 0.127 mm film panel. The data all lie along straight lines, meaning that regardless of film thickness or deflection, the panels still behave in a linear manner for this range of applied loads. In addition, Fig. 5 lacks any indication of disparity in deflection between point 1 and point 2. Although it is still likely that the panels exhibit a saddle configuration under point loading as in the long-side-supported tests, because the points measured are exactly symmetric (Fig. 2), single trend lines are fit to the data in the bottom graphs.

III. Panel Finite Element Data

The prohibitively large size and limited success of large, geometrically accurate, finely meshed, shell element models in numerically simulating the behavior of ultralightweight membrane-dominated space structures [14–17] and the demonstrated linear quasi-static macroscale behavior of panels in the previous section together led to an alternate modeling approach here. Coarsely meshed, single-layered, solid plate shell element models of the panel geometries tested experimentally are described subsequently. The material properties of the solid shell elements were defined to reflect the honeycomb geometry and unique construction of the panels, yielding simple yet accurate models that can be easily applied to all of the experimental cases by modifying the global macroscale geometry [18].

The currently accepted governing equations of lightweight honeycomb-core panels treat the panels in a global sense as Reissner–Mindlin elastic plates. This formulation is based on the classical plate equations solved for selected boundary conditions [12,13]. To apply the Reissner–Mindlin solid plate equations to honeycomb-core panels, various material properties such as shear and rotational moduli and Poisson's ratios must be properly calculated. The derivations of the methods for calculating these properties for honeycombs are listed by Gibson and Ashby [19] and Kelsey et al. [20] and reproduced here.

To approximate the full-panel bending data from Figs. 3–5, simple solid plate finite element models were constructed from four-node shell elements possessing 6 degrees of freedom per node. A simple rectangle matching the length and width dimensions of the rectangular panel in Figs. 1 and 2 was created and meshed with a

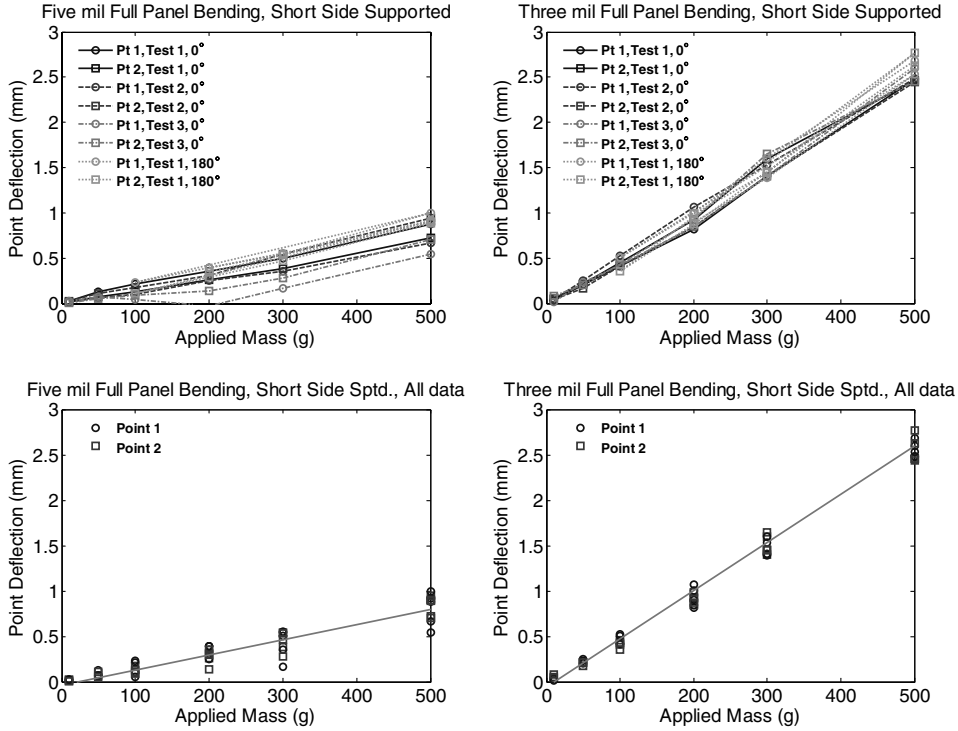

Fig. 5 Short-side-supported full-panel bending data for panels manufactured from both 0.127 mm (5 mil) and 0.0762 mm (3 mil) polyimide film; bottom graphs show the best-fit line.

single layer of shell elements of thickness equal to that of the panel: 40 elements per side. Material properties were defined as regular repeating hexagonal honeycomb panels using Eqs. (1–3) [19,20]:

$$\frac{E_1}{E_s} = \frac{\sigma_1}{\varepsilon_1} = \left(\frac{t}{\ell}\right)^3 \frac{\cos\theta}{(h/\ell + \sin\theta)\sin^2\theta}$$
$$\frac{E_2}{E_s} = \frac{\sigma_2}{\varepsilon_2} = \left(\frac{t}{\ell}\right)^3 \frac{(h/\ell + \sin\theta)}{\cos^3\theta} \tag{1}$$

$$\frac{G_{12}}{E_s} = \left(\frac{t}{\ell}\right)^3 \frac{(h/\ell + \sin\theta)}{(h/\ell)^2(1 + 2h/\ell)\cos\theta} \tag{2}$$

$$\nu_{12} = -\frac{\varepsilon_2}{\varepsilon_1} = \frac{\cos^2\theta}{(h/\ell + \sin\theta)\sin\theta}$$
$$\nu_{21} = -\frac{\varepsilon_1}{\varepsilon_2} = \frac{(h/\ell + \sin\theta)\sin\theta}{\cos^2\theta} \tag{3}$$

where t, h, ℓ, and θ are defined in Fig. 6.

However, honeycomb panels consisting of regular hexagons ($h = \ell$ and $\theta = 30$ deg) are isotropic; therefore [19,21,22],

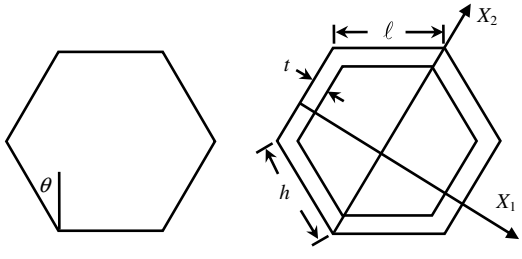

Fig. 6 Geometric parameter definitions for Eqs. (1–3).

$$\frac{E_1}{E_s} = \frac{E_2}{E_s} = 2.3\left(\frac{t}{\ell}\right)^3$$
$$\frac{G_{12}}{E_s} = 0.57\left(\frac{t}{\ell}\right)^3 = \frac{1}{4}\frac{E}{E_s}; \quad \text{and} \quad \nu_{12} = \nu_{21} = 1 \tag{4}$$

Because a Poisson's ratio of 1 creates a situation in which a division by 0 occurs, such as in Eq. (1), Poisson's ratio in the finite element model was set to 0.98.

Unique to these panels and not reflected in the preceding equations, the side walls of the hexagonal voids (stiffeners) that create the honeycomb pattern are not solid polyimide material, but are instead hollow. To incorporate this variation into the existing model without modeling individual cell walls, E_s was modified by performing a virtual tensile test on the hollow sidewalls of the stiff thermal-formed thin-film polyimide panel using Eq. (5), the equation for a beam in axial tension [23]:

$$(EA/L)x = F \tag{5}$$

The value of A was set to match the cross-sectional area of the hollow rectangular sidewalls of the stiffeners in which the thickness of the polyimide film, 0.127 mm (5 mil), was the wall thickness used, and the value of E was set to that of Kapton (2.5 GPa). The values of x were solved for a range of values of F, engineering stress F/A was plotted versus engineering strain x/L, and the slope of the line was calculated, as shown in Fig. 7. This value, called the apparent modulus of a hollow beam, or E_{app}, was used instead of E_s in Eq. (4).

IV. Panel Test/Analysis Correlation

The full-panel shell element models, created using the properties listed in Table 1, were constrained to have zero z displacement along the long edges, loading was applied to the center of the panels, and a nonlinear large-displacement static analysis was run. The results are plotted in Fig. 8 along with the best-fit trend lines from the experimental-panel bending data in Fig. 3. Two different apparent moduli (E_{app}) were used: the smaller of which was calculated using a hollow cross section with sidewalls half as thick as the top and bottom and the greater of which was calculated setting all of the walls

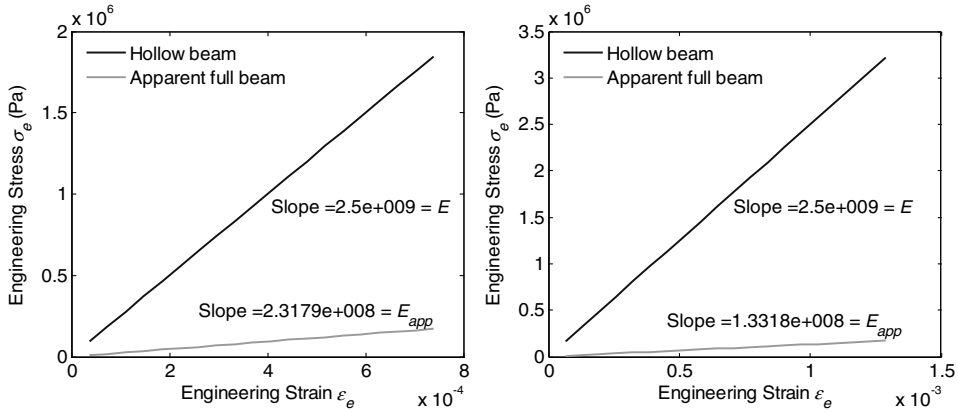

Fig. 7 Virtual tensile test, constant wall thickness (left), sidewall half thickness of top and bottom (right).

of the hollow beam to equal 0.127 mm thickness (Fig. 7). Clearly, the two values chosen for the E_{app} approximation represent the upper and lower bounds between which the true value of E_{app} lies; a different setpoint for E_{app} between the upper and lower bounds would have further improved the fit of the numerical results through the experimental data.

It was noted in the data in Fig. 3 that the two measurement points in the long-side-supported full-panel bending test configuration were not symmetric. Point 1 was located closer to the center of the panel than point 2 (L1 and L2 in Fig. 2), and the fact that it deflected less than point 2 in the data in Fig. 3 indicated that the deformed shape of the panel under point loading was a saddle shape. The data plotted in Fig. 8 for point 1 and point 2 from the finite element model data were also taken from asymmetric points, with point 1 slightly closer to the center of the panel than point 2. The finite element results show the same trends as the experimental data and closely match the experimental results, validating the modeling philosophy of using simple shell elements to model the panels on a global macroscale and negating the need for detailed models of the nonlinear behavior of individual nodes in compression.

The deformed panel from the finite element analysis is shown in Fig. 9, clearly detailing the saddle configuration under point loading.

V. Conclusions

Static bending tests were performed on rectangular, stiff, ultralightweight thin-film polyimide panels manufactured from two different film thicknesses. The results show linear behavior over the entire range of applied loads, demonstrating that previously observed nonlinear static behavior on a small local scale is not present globally. Additionally, other formed-stiffened membrane structures exhibited linear behavior only when pressurized. To reduce model complexity, an apparent modulus for the panels was found by modifying the bulk modulus of the polyimide to account for the unique internal tessellating honeycomb hollow-beam panel structure. A simple coarsely meshed solid plate shell element model using the calculated apparent modulus without reflecting the internal structure of the panel was used to successfully replicate the displacement data and showed that the panels deflect into a saddle configuration under point loading. This model represents a

Table 1 Defined properties for shell element models of a stiff ultralightweight polyimide panel

Panel dimensions	$25.0825 \times 26.67 \times 1.905$ cm
Panel mass	38.3 g
Volumetric density ρ	30.0545 kg/m^3
Areal density	0.57 kg/m^2
Number of elements	1600
Number of nodes	1681
Hexagonal void spacing t	0.3175 cm
Internal hexagon angle θ	30 deg
Hexagon edge length ℓ	$1.27\cos(\theta)$ cm
Poisson's ratio xy, ν_{xy}	0.98
Poisson's ratio xz, ν_{xz}	0.34
Poisson's ratio yz, ν_{yz}	0.34
Apparent modulus E_{app}	1.3318×10^8, 2.3179×10^8 Pa
Major- and minor-axis moduli $E_x = E_y$	$2.3094E_{\text{app}}(t/\ell)^3$

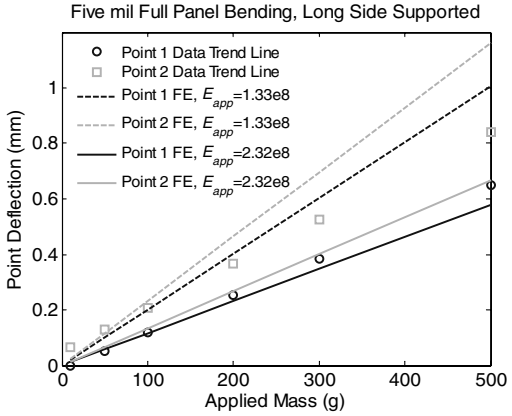

Fig. 8 Full-panel bending models for long-side-supported rectangular panels manufactured from 0.127 mm (5 mil) polyimide film.

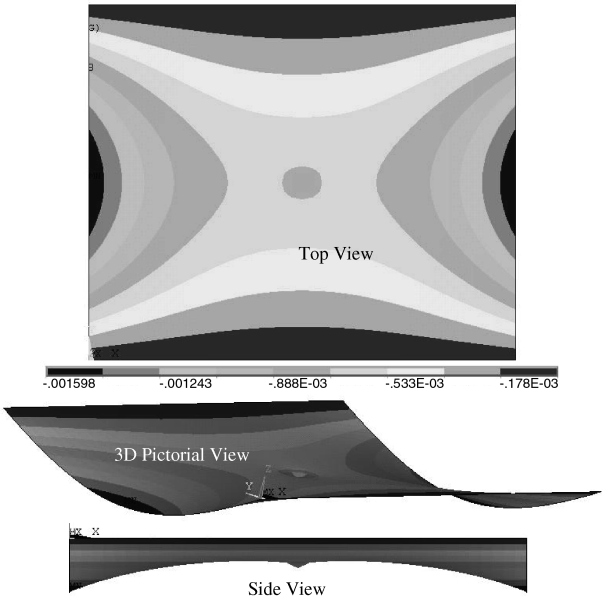

Fig. 9 Deformed shape of the full rectangular panel model manufactured from 0.127-mm-thick (5 mil) polyimide film, scale in meters.

substantial reduction in complexity over previous models of similar structures.

Acknowledgments

This work was performed under a NASA Graduate Student Research Program fellowship, grant number NNL04AA21H (Richard Pappa, advisor), and a NASA Small Business Innovation Research grant (Larry Bradford, principal investigator). This work is a portion of a Ph.D. Dissertation through the University of Kentucky, Jack Leifer and Suzanne Weaver Smith, advisors, and George Blandford and Kozo Saito, committee members.

References

[1] Black, J. T., Smith, S. W., Leifer, J., and Bradford, L. J., "Local Testing and Reduced Model Validation of Thermal-Formed Thin Film Polyimide Panels," *Mechanical Systems and Signal Processing*, Vol. 22, No. 6, Aug. 2008, pp. 1412–1426. doi:10.1016/j.ymssp.2007.11.010

[2] Black, J. T., Smith, S. W., Leifer, J., and Bradford, L., "Measuring and Modeling the Dynamics of Stiffened Thin Film Polyimide Panels," *Journal of Guidance, Control, and Dynamics*, Vol. 31, No. 3, 2008, pp. 490–500. doi:10.2514/1.32236

[3] Black, J. T., "New Ultralightweight Stiff Panels for Space Apertures," Ph.D. Dissertation, Dept. of Mechanical Engineering, Univ. of Kentucky, Lexington, KY, Dec. 2006, http://lib.uky.edu/ETD/ukymeen2006d00532/BlackDis.pdf.

[4] Pappa, R. S., Lassiter, J. O., and Ross, B. P., "Structural Dynamics Experimental Activities in Ultralightweight and Inflatable Space Structures," *Journal of Spacecraft and Rockets*, Vol. 40, No. 1, 2003, pp. 15–23. doi:10.2514/2.3934

[5] Pappa, R. S., Black, J. T., Blandino, J. R., Jones, T. W., Danehy, P. M., and Dorrington, A. A., "Dot Projection Photogrammetry and Videogrammetry of Gossamer Space Structures," *Journal of Spacecraft and Rockets*, Vol. 40, No. 6, 2003, pp. 858–867. doi:10.2514/2.7047

[6] Johnston, J. D., Blandino, J. R., and McEvoy, K. C., "Analytical and Experimental Characterization of Gravity Induced Deformations in Subscale Gossamer Structures," *Journal of Spacecraft and Rockets*, Vol. 43, No. 4, 2006, pp. 762–770. doi:10.2514/1.14298

[7] Flint, E., Bales, G., Glaese, R., and Bradford, R., "Experimentally Characterizing the Dynamics of 0.5 m^+ Diameter Doubly Curved Shells Made From Thin Films," AIAA Paper 2003-1831, April 2003.

[8] Flint, E. M., Lindler, J. E., Hall, J. L., Rankine, C., and Regelbrugge, M., "Overview of Form Stiffened Thin Film Shell Characteristic Behavior," AIAA Paper 2006-1900, May 2006.

[9] Song, H., Smith, S. W., and Main, J. A., "Dynamic Testing of an Inflatable, Self-Supporting, Unpressurized Thin Film Torus," *Journal of Guidance, Control, and Dynamics*, Vol. 29, No. 4, 2006, pp. 839–845. doi:10.2514/1.16509

[10] Griffith, D. T., and Main, J. A., "Experimental Modal Analysis and Damping Estimation of an Inflated Thin-Film Torus," *Journal of Guidance, Control, and Dynamics*, Vol. 25, No. 4, 2002, pp. 609–617. doi:10.2514/2.4934

[11] Ruggiero, E. J., Park, G., and Inman, D. J., "Multi-Input Multi-Output Vibration Testing of an Inflatable Torus," *Mechanical Systems and Signal Processing*, Vol. 18, No. 5, 2004, pp. 1187–1201. doi:10.1016/j.ymssp.2004.01.003

[12] Timoshenko, S., and Woinowsky-Krieger, S., *Theory of Plates and Shells*, McGraw–Hill, New York, 1959.

[13] Reddy, J. N., *Theory and Analysis of Elastic Plates*, Taylor and Francis, Philadelphia, 1999..

[14] Lore, K., and Smith, S. W., "Efficient Computation of Dynamic Response of Large Flexible Spacecraft," AIAA Paper 2005-2051, Apr. 2005.

[15] Wang, J. T., and Johnson, A. R., "Deployment Simulation of Ultra-Lightweight Inflatable Structures," AIAA Paper 2002-1261, 2002.

[16] Tesseler, A., Sleight, D. W., and Wang, J. T., "Nonlinear Shell Modeling of Thin Membranes with Emphasis on Structural Wrinkling," AIAA Paper 2003-1931, 2003.

[17] Su, X., Abdi, F., Taleghani, B., and Blandino, J. R., "Wrinkling Analysis of a Kapton Square Membrane Under Tensile Loading," AIAA Paper 2003-1985, 2003.

[18] Reissner, E., "On Bending of Elastic Plates," *Quarterly of Applied Mathematics*, Vol. 5, 1947, pp. 55–68.

[19] Gibson, L. J., and Ashby, M. F., *Cellular Solids: Structures and Properties*, Pergamon, New York, 1988.

[20] Kelsey, S., Gellatly, R. A., and Clark, B. W., "The Shear Modulus of Foil Honeycomb Cores, A Theoretical and Experimental Investigation on Cores Used in Sandwich Construction," *Aircraft Engineering*, Vol. 30, No. 10, 1958, pp. 294–302. doi:10.1108/eb033026

[21] Hoffman, G. A., "Poisson's Ratio for Honeycomb Sandwich Cores," Rand Corp., Rept. P-946, Santa Monica, CA, 1957.

[22] Horvay, G., "Bending of Honeycombs and of Perforated Plates," *Journal of Applied Mechanics*, Vol. 74, 1952, pp. 122–123.

[23] Craig, R. R., *Structural Dynamics: An Introduction to Computer Methods*, Wiley, New York, 1981.

G. Agnes
Associate Editor